

Deviations from Perfect Memory in Spin Glass Temperature Cycling Experiments

M. Sasaki¹, V. Dupuis², J.-P. Bouchaud² and E. Vincent²

¹ Laboratoire de Physique Théorique et Modèles Statistiques, bât. 100, Université Paris-Sud, F-91405 Orsay, France

² Service de Physique de l'État Condensé, Orme des Merisiers — CEA Saclay, 91191 Gif sur Yvette Cedex, France.

March 7, 2019

Abstract. We study the deviations from perfect memory in negative temperature cycle spin glass experiments. It is known that the a.c. susceptibility after the temperature is raised back to its initial value is superimposed to the reference isothermal curve for large enough temperature jumps ΔT (perfect memory). For smaller ΔT , the deviation from this perfect memory has a striking non monotonous behavior: the ‘memory anomaly’ is *negative* for small ΔT 's, becomes positive for intermediate ΔT 's, before vanishing for still larger ΔT 's. We show that this interesting behavior can be reproduced by simple Random Energy trap models. We discuss an alternative interpretation in terms of droplets and temperature chaos.

PACS. 75.50.Lk Spin glasses and other random magnets – 05.70.Fh Phase transitions: general studies – 64.70.Pf Glass transitions

1 Introduction

It is well known that in glassy systems, dynamical effects strongly depend on the history of the system after quenching from above the glass transition temperature T_g . These phenomena are called aging and have been studied using various experimental protocols[1,2,3]. The measurement of the ac-susceptibility during negative T -cycles is one of them. This experiment consists of the following three stages. In the first stage, the system is quenched from above its critical temperature T_g and it is kept at a temperature T_1 ($< T_g$) during a time t_{w1} . In the second stage the temperature is temporally reduced to $T_2 = T_1 - \Delta T$ during a time t_{w2} , and then it is set back to T_1 in the third stage. The ac-susceptibility (magnetic, dielectric, mechanical,...) is measured during all the three stages. The effect of the perturbation of the temperature is examined by comparing the perturbed and unperturbed (i.e. $t_{w2} = 0$) data in the third stage. From this comparison, it is revealed that the perturbed data quickly approaches the unperturbed one as if the system remembers how far the relaxation at the temperature T_1 had proceeded before the perturbation, even though the system is strongly *rejuvenated* at temperature T_2 (see Fig. 1). This phenomenon is called the memory effect, and has been observed in many glassy systems like spin glasses[4,5,6,7], orientational glasses[8,9,10], polymer glasses[11], etc.

In the present paper, we focus on the deviations from perfect memory that are observed immediately after heating back the system to T_1 . Surprisingly, systematic exper-

iments (that we report in section 2) show that the transient behavior is non monotonous as a function of ΔT . The initial extra contribution, that we will call the memory anomaly, is found to be *negative* for small ΔT , then *positive* for intermediate ΔT , before vanishing completely for large enough ΔT (perfect memory).

We then measure the ac-susceptibility for a T -cycle in the Random Energy Model (REM)[12] or the Generalized REM (GREM)[13]. These models have been shown[14,15,16,17,18,19] to reproduce many of the experimental features of aging, including rejuvenation and memory. We find that the non monotonous transients mentioned above can also be obtained in such models.

Technically, we first establish a relation between the ac-susceptibility and the distribution of relaxation times. Although this relation could not be derived analytically, numerical tests suggest that this relation holds with high accuracy. This enables us to measure the ac-susceptibility for any desired time scale in the REM (but not in the GREM), allowing us to measure the ac-susceptibility in the REM up to time scales comparable to experiments. This would not be possible using Monte Carlo simulations. As for the GREM, the ac-susceptibility is obtained using Monte Carlo simulation, and therefore corresponds to rather small time scales. Our numerical measurements are made for various sets of parameters, i.e., the waiting times t_{w1} and t_{w2} , the temperatures T_1, T_2 and the period of the applied ac-field $P = 2\pi/\omega$. We find that the non monotonous effect described above depends quite sensitively on some of these parameters.

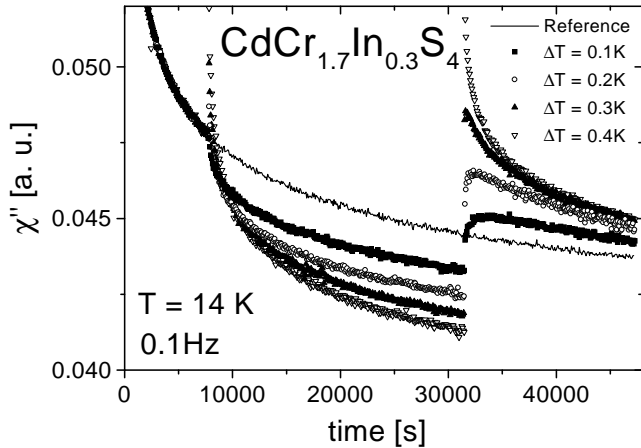


Fig. 1. Out-of-phase susceptibility χ'' vs. time for temperature cycling experiments at $T_1 = 14K$ on the $CdCr_{1.7}In_{0.3}S_4$ Heisenberg spin glass ($T_g = 16.7K$). The sample was quenched to T_1 , kept at this temperature during $t_1 = 7700s$, and then submitted to a negative temperature cycle at $T_1 - \Delta T$ during $t_2 = 23650s$ before returning to T_1 for a time t_3 . Four different small ΔT (0.1K-0.4K) were used.

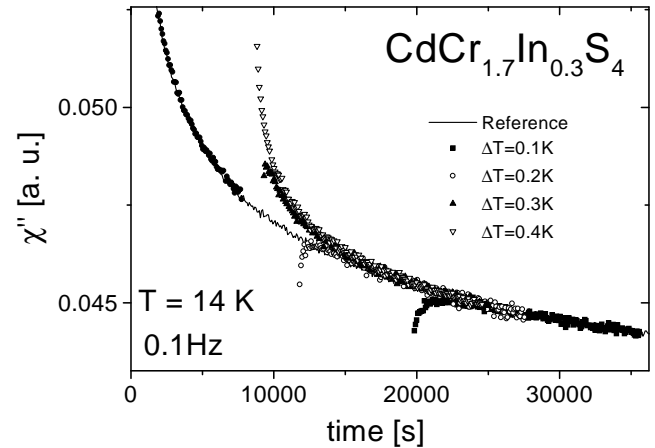


Fig. 2. Superposition of χ'' -relaxations of Fig.1 after the negative temperature cycles onto a reference isothermal relaxation curve (solid line). The data measured after the cycle have been shifted horizontally by $t_2 - t_{eff}$ to take into account the effective contribution t_{eff} of aging at $T_1 - \Delta T$ on aging at T_1 . The merging of the data points with the reference curve occurs first from below for small ΔT 's and then from above for larger ΔT 's.

The organization of this manuscript is as follows: In section 2 results of new complete set of T -cycle experiments in spin glasses are shown. In section 3 we explain the REM, the GREM and the dynamics employed for these models. In section 4 a relation between ac-susceptibility and distribution of relaxation times is proposed and its validity is tested numerically. In section 5 and 6 results on the REM and on the GREM are shown. Finally, in section 7, we give a physical discussion of our results and a comparison with the scenario of temperature chaos, where the existence of an overlap length is assumed.

2 Results of Experiments

The effect of temperature changes on aging has already been largely investigated experimentally in spin glasses [1]. Here we focus on the details of the experimental results in the well characterized thiospinel $CdCr_{1.7}In_{0.3}S_4$ ($T_g = 16.7K$) Heisenberg spin glass sample. Fig. 1 presents the results on the out-of-phase component of χ'' of the a.c. susceptibility during the temperature cycle described in the introduction, with $T_1 = 14K$, for four ΔT values in the range (0.1K-0.4K), and a frequency 0.1 Hz. Note that the period of the a.c. field (10 sec) is typically much larger than any microscopic time scale (10^{-12} sec).¹

Just after the initial quench, χ'' is slowly relaxing downward with time t_{w1} due to aging. When T_1 is decreased to $T_2 = T_1 - \Delta T$, we observe a jump and a strong relaxation in χ'' : this is the rejuvenation effect. Despite this strong reinitialization of aging at $T_1 - \Delta T$, it is possible,

¹ The relevant ‘microscopic’ time scale may however be strongly renormalized by critical fluctuations, as recently discussed in refs. [7,20,21], and can be much larger than 10^{-12} sec. for T close to T_g .

when the temperature is raised back to T_1 and for large enough ΔT ($\geq 2K$) [4], to find a perfect memory of the past relaxation at T_1 . For large ΔT 's, the relaxations at T_1 before and after the temperature cycle are in exact continuity and there is no contribution of aging at $T_1 - \Delta T$ on aging at T_1 . In contrast, in the regime of small ΔT 's of Fig. 1, we do not find a perfect memory of aging after the temperature cycle. The χ'' relaxations after the negative cycle can still be superposed, apart from a transient contribution to be analyzed below, onto a reference isothermal relaxation at T_1 but we now need to shift the data by an effective time $t_{eff} < t_{w2}$ which accounts for aging during the stay at T_2 (see Fig. 2). This effective time t_{eff} has been recently studied in detail both experimentally[7, 21] and numerically[22,23].

Coming back to the transient contribution, we see that for the smallest $\Delta T = 0.1K$ and $0.2K$ used, χ'' reaches a maximum as a function of time, and merges back with the reference curve from below, while for $\Delta T = 0.3K$ and $0.4K$ the maximum disappears and this return occurs from above. This is a systematic effect which is also observed at other temperatures. We have further characterized this feature by gathering the results of several negative temperature cycling experiments done on the thiospinel sample at two temperatures $T_1 = 12K$ and $T_1 = 14K$ and for various ΔT 's. In Fig. 3, we have plotted the (relative) memory ‘anomaly’ $\Delta\chi''/\chi''$, where $\Delta\chi''$ is the difference between the χ'' -value just after the cycle and the one corresponding to an isothermal aging at T during $t_{w1} + t_{eff}$, as a function of $\Delta T/T_1$ for the whole set of available experimental results. The characteristic time scales are given in Tables 1 and 2.

For small ΔT 's, $\Delta\chi''/\chi''$ is negative and χ'' approaches the reference curve from below. As ΔT increases, this ratio becomes positive meaning that the approach takes place now from above the reference curve (Fig. 2). For larger

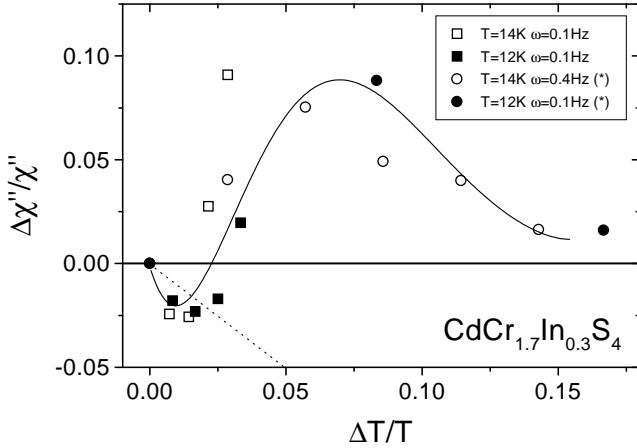


Fig. 3. Relative difference (memory ‘anomaly’) $\Delta\chi''/\chi''$ between the χ'' -value after a negative temperature cycle of amplitude ΔT at a temperature T and the χ'' -value after a corresponding isothermal aging at T during a time $t_1 + t_{\text{eff}}(\Delta T)$ for various temperature cycling experiments (such as the ones presented in Fig.1-2). The first cycles at 14K and 12K (0.1Hz) correspond to $t_1 = 7700\text{s}$ and $t_2 = 23650$. The others (*) correspond to $t_1 = t_2 = 3600\text{s}$ for 14K (0.4Hz) and $t_1 = t_2 = 18000\text{s}$ for 12K (0.1Hz). The thin line is a guide for the eye. The dotted line corresponds to $\Delta\chi''/\chi'' = -\Delta T/T$.

ΔT (K)	t_{eff} (sec)	t^* (sec)	t_{erase} (sec)	$\Delta\chi''/\chi''$
0.1	15000	1200	2850	-1.8×10^{-2}
0.2	8000	1200	2700	-2.3×10^{-2}
0.3	4000	800	475	-1.7×10^{-2}
0.4	2700	–	5300	2.0×10^{-2}

Table 1. Shift time t_{eff} , position of the maximum of χ'' t^* , time at which the signal merges with the shifted reference curve t_{erase} , and memory anomaly $\Delta\chi''/\chi''$ for different ΔT 's, for $T_1 = 12$ K.

ΔT (K)	t_{eff} (sec)	t^* (sec)	t_{erase} (sec)	$\Delta\chi''/\chi''$
0.1	12000	1800	4200	-2.4×10^{-2}
0.2	4000	900	550	-2.6×10^{-2}
0.3	1500	160	8000	2.8×10^{-2}
0.4	1000	–	10350	9.1×10^{-2}

Table 2. The same table as Table 1 for $T_1 = 14$ K.

ΔT 's, $\Delta\chi''/\chi''$ shows a maximum and decreases back towards zero. Beyond that point, rejuvenation and full memory effects are observed [24] and aging at T_2 has no influence on the aging at T_1 . This characteristic oscillation of $\Delta\chi''/\chi''$ as a function of ΔT is the central result of this paper, that we discuss below in the context of Random Energy Models.

Note furthermore that the time at which the maximum of χ'' occurs rapidly decreases as ΔT increases, whereas the time t_{erase} at which the signal merges with the shifted reference curve has a non monotonic behavior with ΔT (see Tables 1 and 2). For still larger ΔT 's, this time decays back to zero.

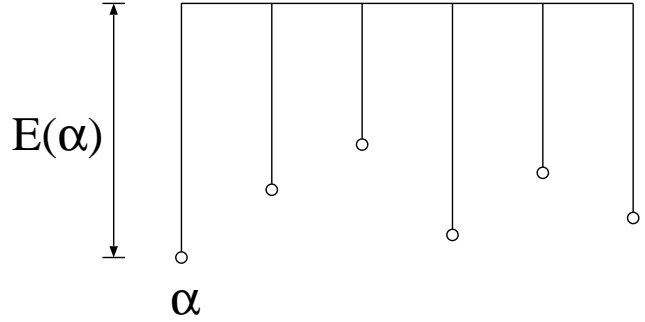


Fig. 4. Structure of the Random Energy Model.

3 Models

This section is devoted to introducing the REM, the GREM and their dynamical extensions. A magnetization-like variable is introduced in order to define and measure an ac-susceptibility.

3.1 The REM

The REM is schematically shown in Fig. 4. The bottom points are the accessible states of the system. We will consider the case where N , the total number of states, is very large. Each branch represents the barrier energy E , over which the system goes from one state to another. The values of E are assigned randomly and independently according to the distribution :

$$\rho(E)dE = \frac{dE}{T_g} \exp[-E/T_g] \quad (E \geq 0), \quad (1)$$

where T_g is the transition temperature of the model. Hereafter T_g is used as the unit of temperature and is set to 1.

From the Arrhenius law, the escape time $\tau(\alpha)$ is related to $E(\alpha)$ as

$$\tau(\alpha) = \tau_0 \exp[E(\alpha)/T], \quad (2)$$

where T is the temperature and τ_0 is a microscopic time scale. Hereafter τ_0 is used as the unit of time and is set to 1. From eq. (1), the distribution of τ is

$$p_x(\tau)d\tau = \frac{x}{\tau^{x+1}}d\tau \quad (\tau \geq 1), \quad (3)$$

where $x \equiv T/T_g$. From eq. (3), it is clear that the averaged relaxation time is $x/(x-1)$ for $x > 1$ and infinite for $x \leq 1$. This means that the transition from an ergodic phase to a non-ergodic phase occurs at T_g [14].

We define the dynamics of the REM from a simple Markoff process that defines a ‘trap’ model (see also [25]). At $t = 0$, an initial state β is chosen according to the uniform distribution over all states, i.e.,

$$P_\alpha(0) = \frac{1}{N}. \quad (4)$$

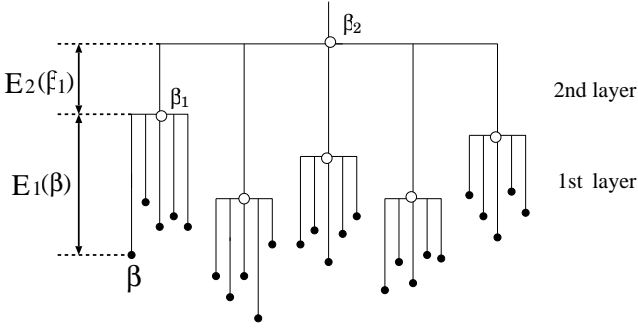


Fig. 5. Structure of the Generalized Random Energy Model with $L = 2$.

This means that the system is quenched from an infinitely high temperature. After the initial state is chosen, the system successively changes its state by repeating the following two processes.

1. The system is activated from the present state β with probability $\tau(\beta)^{-1}$ per unit time.
2. After the activation from β , the system falls in one of all the states with uniform probability.

When a magnetic field $H(t)$ is applied, the energy of a state β is shifted by $-H(t)M_\beta$ and the activation energy changes from $E(\beta)$ to $E(\beta) + H(t)M_\beta$, where M_β is the magnetization of a state β . This is the only effect of the magnetic field that we consider. The values of the magnetizations M_β are assigned randomly and independently from a given distribution $D(M)$ with zero mean.

3.2 The GREM

The GREM is schematically shown in Fig. 5. This model is generated by piling up L different REM's in a hierarchical way. The Energy of a branch in the n -th layer (n is counted from the bottom), E_n , are given according to the distribution

$$\rho_n(E_n)dE_n = \frac{dE_n}{T_g(n)} \exp[-E_n/T_g(n)] \quad (E_n \geq 0). \quad (5)$$

The transition temperatures for the layers are chosen so as to satisfy

$$T_g(1) < T_g(2) < \dots < T_g(L). \quad (6)$$

Therefore, in this model, the system freezes progressively from the uppermost (the L -th) layer to the lowest one as the temperature decreases.

Now let us turn to the dynamics of the GREM. The initial state is given in the same way as the REM, i.e., eq. (4). After the initial state is chosen, the system successively changes its state by repeating the following two processes.

1. The system is activated from the present state β to its k -th ancestor β_k (see Fig. 5) with the probability

$$W(\beta; k) = \left[\tau_0^{-1} \prod_{i=1}^k \exp[-E_i(\beta_{i-1})/T] \right] \times \left[1 - \exp[-E_{k+1}(\beta_k)/T] \right], \quad (7)$$

per unit time. By convention, $E_{L+1}(\beta_L) \equiv \infty$. The first factor in the right hand represents the probability that the system is activated from β to β_k and the second one insures that the transition from β_k to β_{k+1} is not active.

2. After the activation from β to β_k , the system falls to one of all the states “under” β_k with uniform probability.

When magnetic field $H(t)$ is applied, $E_1(\beta)$ in eq. (7) is replaced by $E_1(\beta) + H(t)M_\beta$. In order for nearby states to have strongly correlated magnetizations, the value of magnetization of a state β is assigned to be

$$M_\beta = \mathcal{M}_1(\beta) + \mathcal{M}_2(\beta_1) + \dots + \mathcal{M}_L(\beta_{L-1}), \quad (8)$$

where $\mathcal{M}_{k+1}(\beta_k)$ is the contribution from the branching point β_k . The value of \mathcal{M}_k is assigned independently and randomly from a given distribution $D_k(\mathcal{M}_k)$ with zero mean. If the distance $d(\alpha, \beta)$ between α and β is k , i.e., $\alpha_n = \beta_n$ for $n \geq k$, the correlation between M_α and M_β comes from the common contributions of \mathcal{M}_n ($n \geq k+1$) to these magnetizations, and is given by

$$\overline{M_\alpha M_\beta} = \sum_{n=k+1}^L \overline{\mathcal{M}_n^2}, \quad (9)$$

where $\overline{\mathcal{M}_n^2}$ is the variance of $D_n(\mathcal{M}_n)$. It decreases monotonically as k increases and thus as the barrier between the two states becomes higher, just as occurs in the SK model[26].

4 Estimates of the a.c.-susceptibility

Before we show our results, let us explain how we measure the ac-susceptibility. One simple way is to perform a Monte Carlo simulation. But time scales for which we can study by Monte Carlo simulation is quite different from the experimental one. For example, if we measure the period of the applied ac-field in units of the microscopic time of the system, a typical value in numerical studies is 10^2 (see refs. [16, 19, 22, 27, 28]), while that in experiments is $10^6 - 10^{12}$ (in the vicinity of T_g , the microscopic time scale may be renormalized by critical fluctuations: see refs. [4, 5, 7]).

In the case of the REM, we can overcome this problem by using the relation

$$\chi(\omega, t) \approx \frac{\overline{M^2}}{T} \int \frac{1}{1 - i\omega\tau} Q(\tau, t) d\tau, \quad (10)$$

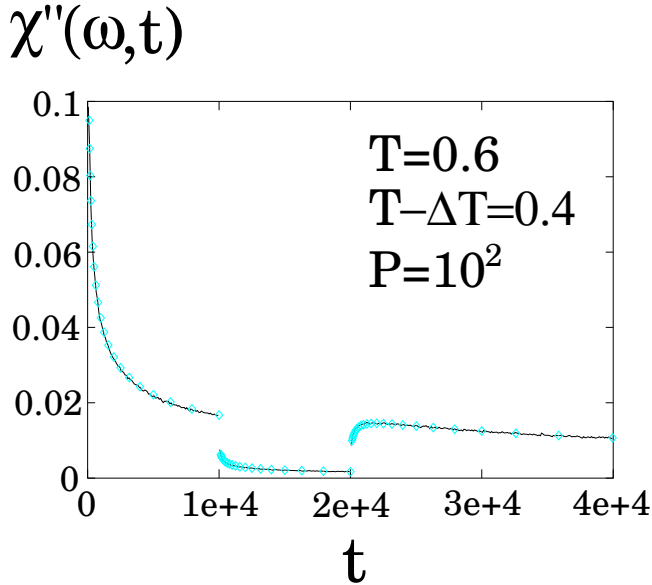


Fig. 6. The REM out-of-phase ac-susceptibility $\chi''(\omega, t)$ after a negative T -cycle. It is measured in two different ways. One can measure $\chi''(\omega, t)$ directly by a Monte Carlo simulation (the lines). The another way is to measure $\chi''(\omega, t)$ using the relation eq. (10) (the diamonds). After the system is quenched from an infinitely high temperature, the temperature is changed as $T_1 = 0.6 \rightarrow T_2 = 0.4 \rightarrow T_1$. The period of the applied ac-field P is 100. For the data obtained by Monte Carlo simulation, an average is taken over 2×10^7 samples.

where ω is the angular frequency of the ac-field, $\overline{M^2}$ is the variance of $D(M)$ and $Q(\tau, t)$ is the probability density that the system is found at time t in one of the states whose relaxation time is τ . In eq. (10), both $\chi(\omega, t)$ and $Q(\tau, t)$ are the disorder averaged quantities. The merit of this method is that we can calculate $Q(\tau, t)$ at arbitrary time t for arbitrary initial condition $Q(\tau, t = 0)$ because the Green function $G_{\beta\alpha}(t)$, i.e., the probability that the system which initially is at α reaches β at time t , has already been calculated analytically in ref. [15]. As a result, we can estimate ac-susceptibility even for very long time scales comparable to those in experiments. The details of how we can calculate $Q(\tau, t)$ are described in the appendix.

Here the question is whether the relation eq. (10) is valid or not even if the system is not equilibrated. In order to examine this question, we compared data obtained by Monte Carlo simulation and those obtained by eq. (10). One example is shown in Fig. 6. A negative T -cycle is applied during the measurement. The agreement between both data is almost perfect. We also checked that both data coincide very well also for the in-phase ac-susceptibility χ' . We can therefore trust the validity of eq. (10) for our purposes.

Concerning the GREM, $\chi(\omega, t)$ has been measured by Monte Carlo simulation because we have not succeeded in calculating $Q(\tau, t)$ analytically.

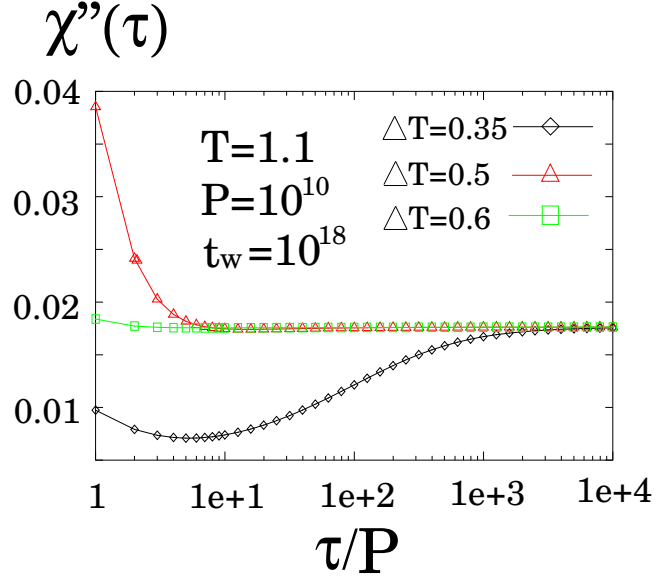


Fig. 7. The REM out-of-phase ac-susceptibility χ'' after a negative T -cycle, plotted as a function of τ/P , where τ is the time elapsed after the temperature is returned to T_1 and P is the period of the applied ac-field. After the system is quenched from an infinitely high temperature, it is kept at $T_1 = 1.1$ for $t_w = 10^{18}$. Then the temperature is reduced to $T_1 - \Delta T$ for t_w , and is then shifted back to T_1 . The period of the applied ac-field is $P = 10^{10}$.

5 Results for the REM

In this section, the results of ac-susceptibility measurements during a T -cycle in the REM are shown. The measurement is done in the following way: After the system is quenched from an infinitely high temperature, the temperature is kept at T_1 in the first stage. In the subsequent second stage the temperature is reduced to $T_1 - \Delta T_n$ ($\Delta T_n = 0.025n$), and then it is returned to T_1 in the third stage. The time t_{w1} of the first stage and that of the second stage (t_{w2}) are taken to be equal for simplicity: $t_{w1} = t_{w2} = t_w$. The ac-susceptibility $\chi(\omega, t)$ is estimated by (10) with $\overline{M^2} = 1$.

5.1 The case $T_1 > T_g$

5.1.1 Results

In Fig. 7, out-of-phase ac-susceptibility χ'' for $T_1 = 1.1$ and $t_w = 10^{18}$ is plotted as a function of τ/P , where τ is elapsed time in the third stage and P is the period of the applied ac-field. The value of P is 10^{10} . We find that χ'' approaches its equilibrium value χ''_{eq} from below for small ΔT , it approaches from above for intermediate ΔT , and $\chi'' \approx \chi''_{\text{eq}}$ from the beginning of the third stage for large ΔT . This is exactly what is observed in experiments. In Fig. 8, we plot

$$\Delta\chi'' \equiv \chi''(t = 2t_w + P) - \chi''(t = t_w), \quad (11)$$

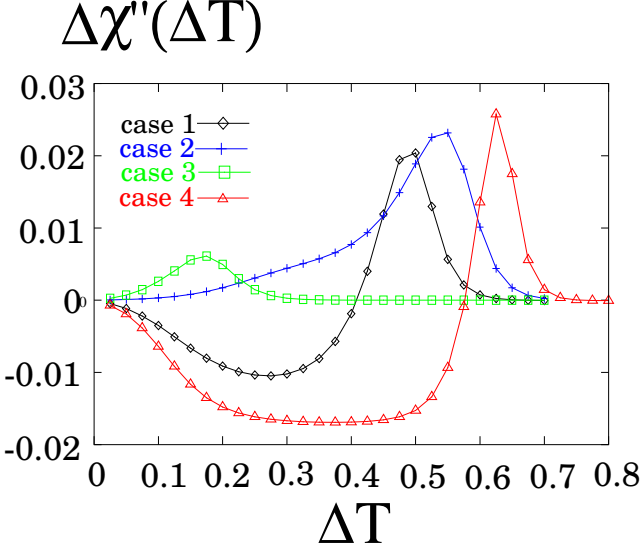


Fig. 8. $\Delta\chi''$ measured in the REM, plotted as a function of ΔT (see eq. (11) for the definition of $\Delta\chi''$). The values of the temperature T_1 , the period of the applied ac-field P and the waiting time t_w are $(T_1, P, t_w) = (1.1, 10^{10}, 10^{18})$ for case 1, $(T_1, P, t_w) = (1.25, 10^{10}, 10^{18})$ for case 2, $(T_1, P, t_w) = (1.1, 10^{15}, 10^{18})$ for case 3 and $(T_1, P, t_w) = (1.1, 10^{10}, 10^{23})$ for case 4.

as a function of ΔT by the diamonds (case 1). We can easily find the similarity between this curve and the experimental one shown in Fig. 3.

Now let us change one of the three parameters T_1 , P and t_w and see how these changes affect the result. First, $\Delta\chi''$ when only T_1 is changed from 1.1 to 1.25 is shown in Fig 8 by the crosses (case 2). The behavior is quite different from that observed in the case 1 above, i.e., $\Delta\chi'' > 0$ for all ΔT 's. Next, $\Delta\chi''$ when only P is changed from 10^{10} to 10^{15} is shown by the squares (case 3). We again find that $\Delta\chi'' > 0$ for all ΔT 's. Finally, $\Delta\chi''$ when only t_w is changed from 10^{18} to 10^{23} is shown by the triangles (case 4). Although the value of ΔT above which $\Delta\chi'' \approx 0$ becomes large, there are not qualitative differences in comparison with case 1. Therefore, the non monotonous transient effect disappears (i) at low frequencies and (ii) when the initial temperature is not close enough to T_g .

5.1.2 Qualitative discussion

In order to understand these surprising results, let us investigate the time dependent energy distribution $P(E, t)$ which is related to $Q(\tau, t)$ through the relation

$$P(E, t)|dE| = Q(\tau, t)|d\tau|, \quad (12)$$

and eq. (2). In Fig. 9, $P(E, t)$ at $t = 2t_w + P$ (i.e. in the third part of the cycle, after one period of the a.c. field) is plotted for six different values of ΔT (the thick line). The parameters T_1 , t_w and P are the same as those of the case 1 in Fig. 8. For comparison, a function which is

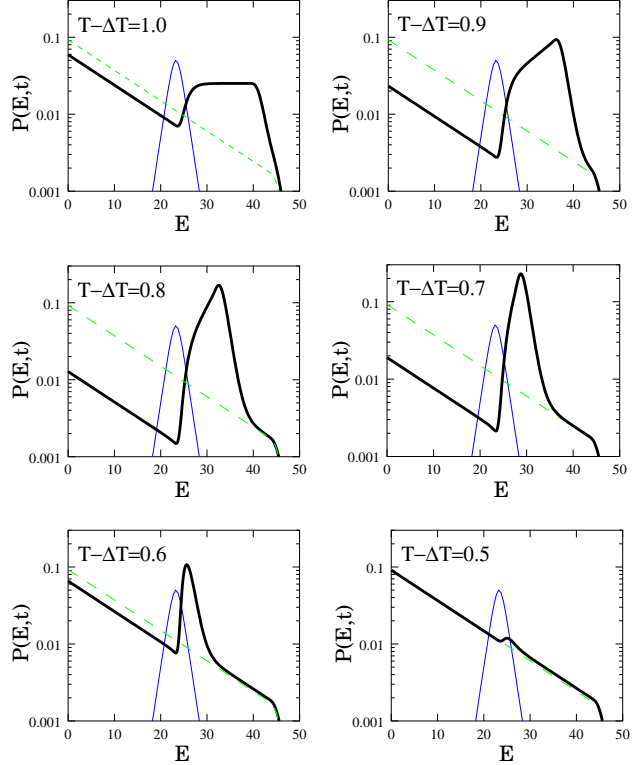


Fig. 9. The energy distribution $P(E, t)$ in the REM at time $t = 2t_w + P$ after a negative T -cycle (the thick line). The values of parameter T , P and t_w are the same as those of the case 1 in Fig. 8. For comparison, a function proportional to $\Omega(E)$ (see eq. (13)) and $P(E, t_w)$ at $t = t_w$ are drawn by the thin line and the broken one, respectively.

proportional to

$$\Omega(E) \equiv \frac{\omega\tau}{1 + (\omega\tau)^2} = \frac{(\frac{2\pi}{P}) \exp(E/T)}{1 + (\frac{2\pi}{P})^2 \exp(2E/T)}, \quad (13)$$

and $P(E, t)$ at $t = t_w$ are drawn by the thin line and the broken one, respectively. It is worth noticing that the data of case 1 in Fig. 8 are obtained by integrating $P(E, t = 2t_w + P)\Omega(E)$ over E . From this figure, we find that $P(E, t)$ has both a minimum and a maximum as a function of E (or a plateau in the special case $T_1 - \Delta T = 1.0$).

When the system is kept at a temperature T for a time t , the equilibration at T proceeds and $P(E, t)$ becomes proportional to $\exp[\lambda_{\text{eq}}(T)E]$ with

$$\lambda_{\text{eq}}(T) = \frac{1}{T} - \frac{1}{T_g}, \quad (14)$$

for $0 \leq E \leq T \log(t)$. Therefore, $P(E, t)$ is equilibrated up to the energy:

$$E_2 \approx (T_2) \log(t_w), \quad (15)$$

in the second stage. When the temperature is returned to T_1 , the re-equilibration at temperature T_1 starts and it

proceeds up to

$$E_3 \approx T \log(P), \quad (16)$$

at time $t = 2t_w + P$. These considerations naturally lead us to the approximate shape of the energy distribution:

$$P(E, 2t_w + P) \propto \begin{cases} \exp[\lambda_{\text{eq}}(T_1)E] & (0 \leq E \leq E_3), \\ \exp[\lambda_{\text{eq}}(T_2)E] & (E_3 \leq E \leq E_2), \end{cases} \quad (17)$$

provided $E_3 < E_2$. Accordingly, a minimum around $E \approx E_3$ and a maximum around $E \approx E_2$ appear for $T_2 < 1.0$, and there is a plateau between E_3 and E_2 for $T_2 = 1.0$. As for the case $T_2 = 0.5$, the peak is erased since in this case $E_2 < E_3$.

From Fig. 9, the result of the case 1 in Fig. 8 is understood as follows. Because of the existence of a peak (or a plateau) and the normalization of $P(E, t)$ with respect to E , the difference $P(E, t = 2t_w + P) - P(E, t = t_w)$ changes its sign at a certain point E_* , which is slightly greater than E_3 . Figure 9 shows that the peak around E_2 grows as ΔT increases. If we take the normalization condition into account, we notice that the growth of the peak means a decrease of $P(E, t = 2t_w + P)$ for $E < E_*$, and a corresponding increase of the quantity $\Delta\chi''_-(\Delta T)$, defined as

$$\Delta\chi''_-(\Delta T) \equiv \int_0^{E_*} dE \Omega(E) \left| P(E, 2t_w + P) - P(E, t_w) \right|. \quad (18)$$

On the other hand, if ΔT is not very large and the location of the peak is not close to E_3 , the second contribution $\Delta\chi''_+(\Delta T)$, defined as:

$$\Delta\chi''_+(\Delta T) \equiv \int_{E_*}^{\infty} dE \Omega(E) \left| P(E, 2t_w + P) - P(E, t_w) \right|, \quad (19)$$

cannot be very large (note that the peak of $\Omega(E)$ is around E_3). As a result, $\Delta\chi'' = \Delta\chi''_+ - \Delta\chi''_-$ is negative for small ΔT (see Fig. 10 where $\Delta\chi''_+(\Delta T)$ and $\Delta\chi''_-(\Delta T)$ for case 1 are plotted by the diamonds). Then, as ΔT increases, the location of the peak approaches E_3 and $\Delta\chi''_+(\Delta T)$ increases. Therefore, $\Delta\chi''(\Delta T)$ is positive for intermediate ΔT . This peak disappears when ΔT is large and $E_2 < E_3$. This is the reason why $\Delta\chi''(\Delta T) \approx 0$ for large ΔT .

Our next interest is to understand the following two trends:

- (i) If either the temperature or the period of the applied ac-field is large enough, $\Delta\chi''(\Delta T) > 0$ for all ΔT .
- (ii) The behavior of $\Delta\chi''(\Delta T)$ does not depend sensitively on t_w , except that the value of ΔT above which $\Delta\chi'' \approx 0$ increases with t_w .

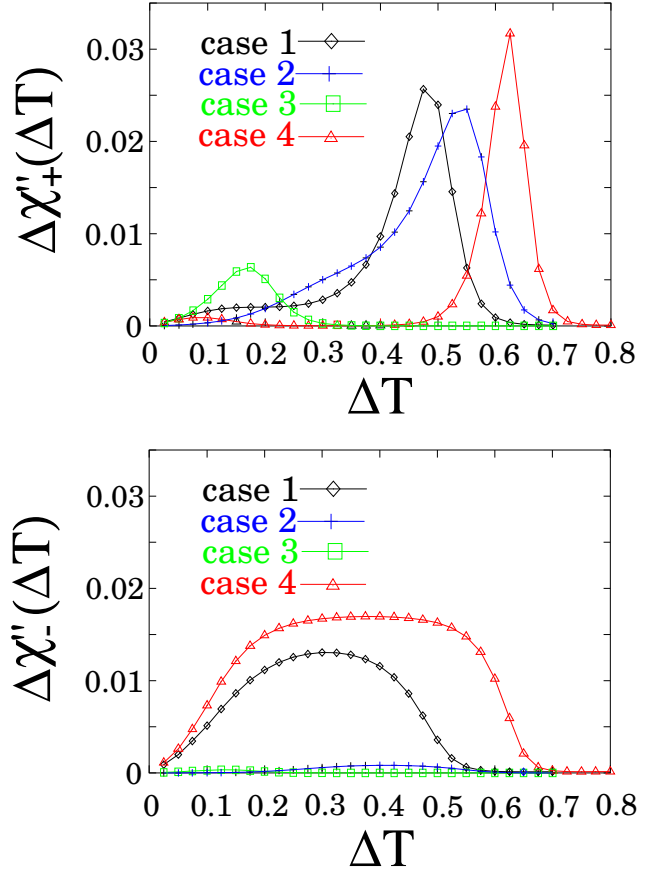


Fig. 10. The functions $\Delta\chi''_+(\Delta T)$ and $\Delta\chi''_-(\Delta T)$ in the REM for each of the cases of Fig. 8 are plotted as a function of ΔT . See eqs. (18) and (19) for the definitions of $\Delta\chi''_+$ and $\Delta\chi''_-$.

To understand these trends, an important point is to note that $\Delta\chi''_-(\Delta T)$ satisfies the inequality

$$\begin{aligned} \Delta\chi''_-(\Delta T) &< \int_0^{\infty} dE \Omega(E) P(E, t = t_w) \\ &\approx \int_0^{\infty} dE \lambda_{\text{eq}}(T) \exp[\lambda_{\text{eq}}(T)E] \Omega(E) \\ &\sim P^{\frac{T_g - T}{T_g}}. \end{aligned} \quad (20)$$

It is obvious from this inequality that $\Delta\chi''_-(\Delta T)$ is a decreasing function of T and P . The quantity $\Delta\chi''_+(\Delta T)$, on the other hand, does not depend strongly on either T or P . This explains point (i) above.

On the other hand, there is no t_w dependence in the inequality (20). This is the reason why behavior of $\Delta\chi''(\Delta T)$ does not depend on t_w so much. However, the value of ΔT above which $\Delta\chi'' \approx 0$ increases with increasing t_w because it is determined from the condition:

$$E_2 \approx E_3. \quad (21)$$

The explanation for these two trends is confirmed by Fig. 10, where $\Delta\chi''_+(\Delta T)$ and $\Delta\chi''_-(\Delta T)$ in each of the cases of Fig. 8 are plotted as a function of ΔT . The function $\Delta\chi''_+(\Delta T)$ does not depend much on the parameters T , P and t_w

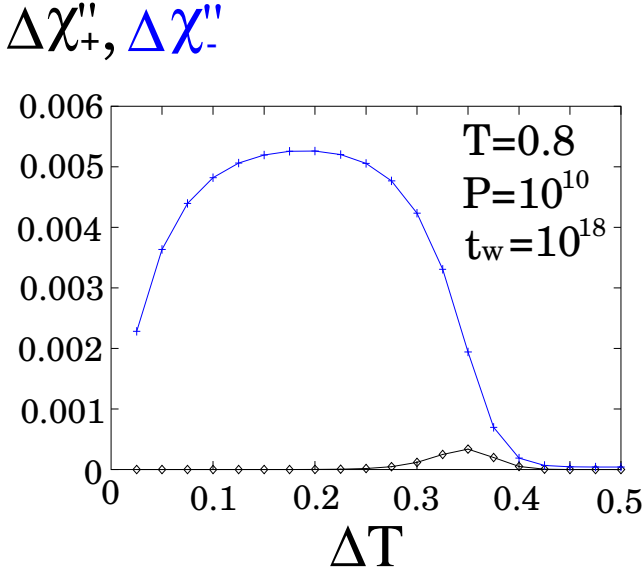


Fig. 11. The functions $\Delta\chi''_+$ (the diamonds) and $\Delta\chi''_-$ (the crosses) in the REM for the case $T_1 = 0.8$, $P = 10^{10}$ and $t_w = 10^{18}$. The definition of $\Delta\chi''_+$ and that of $\Delta\chi''_-$ are slightly changed by replacing $P(E, t = t_w)$ in eqs. (18) and (19) with $P_{\text{const}}(E, t = t_{\text{eff}})$, where $P_{\text{const}}(E, t)$ is isothermal energy distribution at T and t_{eff} is defined by eq. (22).

compared to $\Delta\chi''_-(\Delta T)$, which becomes rather small when either T or P is large enough.

5.2 The case $T_1 < T_g$

Figure 11 shows $\Delta\chi''_+$ and $\Delta\chi''_-$ in the case $T_1 = 0.8$, $P = 10^{10}$ and $t_w = 10^{18}$. Because χ'' decreases towards zero with time for $T < T_g$, we change slightly the definition of $\Delta\chi''_+$ and that of $\Delta\chi''_-$ and replace $P(E, t = t_w)$ in eqs. (18) and (19) with $P_{\text{const}}(E, t = t_{\text{eff}})$, where $P_{\text{const}}(E, t)$ is isothermal energy distribution at T_1 , and t_{eff} is estimated as

$$t_{\text{eff}} = t - t_w + (t_w)^{T_2/T_1}. \tag{22}$$

It is worth noticing that the effective time in the second stage is estimated as $(t_w)^{T_2/T_1}$. It has been shown in ref. [17] that this way to estimate the effective time works well in the REM. The result is similar to that of the case $T_1 > T_g$ shown in Fig. 8 in the sense that $\Delta\chi''_-$ has a wide plateau and $\Delta\chi''_+$ has a peak around the value of ΔT at which eq. (21) is satisfied (in this case the value is about 0.356). The only difference is that $\Delta\chi''_+$ now never exceeds $\Delta\chi''_-$, so that $\Delta\chi''$ is negative for all ΔT .

The dependence on the different parameters was also investigated by changing one of the three parameters T , P and t_w . The ranges we examined are $0.75 \leq T_1 \leq 0.9$, $10^{10} \leq P \leq 10^{15}$ and $10^{18} \leq t_w \leq 10^{23}$, respectively. As a result, we found that $\Delta\chi''_- > \Delta\chi''_+$ is always satisfied for all ΔT in all the cases. Therefore, the condition $T_1 > T_g > T_2$ is required to observe a non monotonous memory anomaly.

6 Results for the GREM

Now let us turn our attention to the GREM. As mentioned in §4, $\chi(\omega, t)$ for the GREM has been measured using Monte Carlo simulation because we have not succeeded in calculating $Q(\tau, t)$ analytically. However, we do not measure $\chi(\omega, t)$ from the linear response to an ac-field because this procedure requires averaging over a very large number of samples (typically $10^7 - 10^8$ samples). Instead, we have estimated the ac-susceptibility from the relations:

$$\chi_k(\omega, t) = \frac{\overline{\mathcal{M}_k^2}}{T} \int \frac{1}{1 - i\omega\tau_k} Q_k(\tau_k, t) d\tau_k, \tag{23}$$

where

$$\tau_k \equiv \exp \left[\frac{\sum_{i=1}^k E_i}{T} \right], \tag{24}$$

the function $Q_k(\tau, t)$ is the probability density of τ_k at time t and $\chi_k(\omega, t)$ is ac-susceptibility calculated from \mathcal{M}_k . It is this probability density $Q_k(\tau_k, t)$ that we obtained from Monte Carlo simulation. The validity of these relations was confirmed numerically by comparing data from the direct measurement of \mathcal{M}_k under an ac-field and from eq. (23).

Because we have to rely on Monte Carlo simulation, the time scales are rather restricted as compared to the REM. Therefore, we will confine ourselves to showing results with one set of parameters. The system we have investigated is the GREM with $L = 2$ (L is the number of layers), $T_g(1) = 0.5$ and $T_g(2) = 1.0$. The disorder average is taken over 8×10^6 samples. The period of the applied ac-field is 300. After the system is quenched from an infinitely high temperature, the temperature is kept at $T_1 = 0.85$ for $t_w = 10^5$ in the first stage. In the subsequent second stage the temperature is reduced to T_2 for t_w , and then it is returned to T_1 in the third stage. In Fig. 12, the contribution from both levels, χ''_1 and χ''_2 are plotted as a function of τ , where τ is elapsed time in the third stage. As for χ''_1 , we again find a non monotonous behavior, similar to that observed in experiments (Fig. 3) and in the REM (Fig. 7). This was expected, since for the first level dynamics is very similar to the single REM, with transitions to the higher level frozen by the fact that $T_1 < T_g(2)$.

On the other hand, the memory anomaly in χ''_2 is always negative, for all values of ΔT . This result is consistent with that obtained in the REM where χ'' always approaches the reference curve from below if $T_1 < T_g$ (note that $T_1 < T_g(2)$ in the present case).

Finally, let us discuss what would happen in the case $L \gg 1$. There, some layers are frozen ($T < T_g(n)$) and others layers are *fast* ($T > T_g(n')$) at any given temperature $T < T_g = T_g(L)$. From the study on the REM shown in §5, we expect that the contributions to χ'' from the frozen layers will always lead to a negative memory anomaly, where as the contribution from the ‘critical’ levels will lead to a non monotonous contribution.

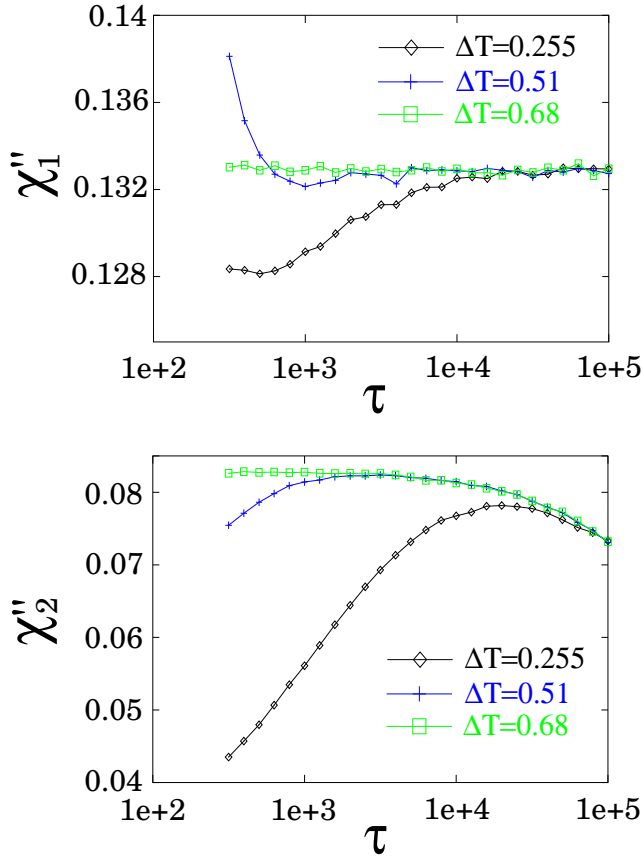


Fig. 12. The GREM out-of-phase ac-susceptibility χ''_k after a negative T -cycle as a function of the elapsed time τ after the temperature is returned to T_1 . This GREM has $L = 2$, $T_g(1) = 0.5$ and $T_g(1) = 1.0$. The period of the applied ac-field is $P = 3 \times 10^2$. After the system is quenched from an infinitely high temperature, the temperature is kept at $T_1 = 0.85$ for $t_w = 10^5$ in the first stage. In the second stage the temperature is temporally reduced to $T_1 - \Delta T$ for the same time t_w , and before being returned to T_1 in the last stage.

7 Discussion. Other scenarios

We have seen that the non monotonous transient effect observed in memory experiments can be reproduced within simple REM trap model, provided the temperature is above and close enough to the critical temperature and the frequency not too low. The same mechanism is present in the GREM, and is governed by the dynamics around the ‘critical level’, i.e. the level such that its critical temperature is close to the working temperature. As emphasized in refs. [29,20], the physical interpretation of the different ‘levels’ is in terms of length scales: small scale dynamics corresponds to the deepest level of the tree, whereas large length scales correspond to the upper level of the trees. The observed aging dynamics always concerns those length scales (levels) around the critical temperature: larger length scales are frozen, whereas smaller length scales are completely equilibrated. Hence, in the above GREM interpretation, the important ingredient is that the system remains close to criticality at any temperature, but the basic ingredient is already present in

the REM, and is related to the abrupt change of the way the different states are explored at T_g (see [30]).

The GREM model is a concrete implementation of the so called ‘hierarchical’ interpretation of experimental data [31], to which one often opposes the ‘droplet’ interpretation [32]. As discussed in details in refs. [20], the two interpretations are to some extent complementary if one wants to interpret the ‘hierarchy’ of phase space as a hierarchy of length and time scales. However, the droplet interpretation of the rejuvenation and memory experiments makes an extra assumption. The existence of an overlap length $\ell_{\Delta T}$ between typical configurations at T and $T - \Delta T$ is postulated [33,32], such that for length scales larger than $\ell_{\Delta T}$, the configurations at the two temperatures are completely unrelated (‘temperature chaos’). Using plausible arguments, one deduces that $\ell_{\Delta T}$ should diverge as a power-law of ΔT for $\Delta T \rightarrow 0$. After a waiting time t_{w1} , the active length scales are such that $\tau_r(\ell_{w1}, T_1) \sim t_{w1}$, where $\tau_r(\ell, T)$ is the typical relaxation time corresponding to length ℓ at temperature T . Length scales much smaller than ℓ_{w1} are fully equilibrated. In this picture, the scenario for rejuvenation is thus the following: whenever $\ell_{w1} < \ell_{\Delta T}$, the temperature change does not modify the achieved pattern, but only acts to slow down the dynamics. Conversely, when ΔT is such that $\ell_{w1} > \ell_{\Delta T}$, the system has to start rebuilding new correlations as if it were brought directly from high temperature (when $\ell_{\Delta T} \rightarrow 0$). As shown in details in refs. [34], this does not necessarily mean that the structure grown at the first temperature is immediately washed away. On the contrary, as long as the length scales ℓ_{w2} , active at T_2 , remain small compared to ℓ_{w1} , memory can be partially or totally recovered. The criterion is the following: the time needed to erase the effect of the dynamics at T_2 when the system is heated back is given by:

$$t_{\text{erase}}(t_{w2}) \sim \tau_r(\ell_{w2}, T_1). \quad (25)$$

Since ℓ_{w2} decreases extremely fast with decreasing temperature [20, 7, 23, 21, 35], $t_{\text{erase}}(t_{w2})$ decreases very rapidly (for a given t_{w2}) as ΔT increases, and should soon becomes smaller than ω^{-1} , which is the smallest time for which a measurement of the a.c. susceptibility can be performed. When $t_{\text{erase}}(t_{w2}) > \omega^{-1}$, on the other hand, one expects to see an initial spike in the a.c. susceptibility that corresponds to the reconstruction of small length scale correlations at T_1 . Schematically, the temperature chaos scenario therefore predicts that the memory anomaly $\Delta\chi$ should be zero for $\Delta T < \Delta T^*$, with $\ell_{w1} = \ell_{\Delta T^*}$, positive for larger ΔT , but becoming zero again when $t_{\text{erase}}(t_{w2})$ becomes shorter than ω^{-1} .

One can finally argue that the number of thermally active (equilibrium) droplets decreases slightly when the temperature is reduced from T_1 to T_2 , thereby reducing the equilibrium a.c. susceptibility. The need to re-nucleate these droplets back at T_1 , which also takes a time $\sim t_{\text{erase}}$, would then explain the negative contribution to the memory anomaly for small ΔT .² This would predict that

² Note that the negative initial contribution to $\Delta\chi$ is like the Kovacs effect in polymeric glasses [37,23].

$\Delta\chi''/\chi''_{\text{eq}} \simeq -[1/T + |\mathcal{Y}'/\mathcal{Y}|]\Delta T$ for small ΔT , where \mathcal{Y} is the temperature dependent stiffness of the droplets. The experimental effect, found to be stronger than $-\Delta T/T$, is in qualitative agreement with this prediction (see Fig. 3). We have furthermore checked that the amplitude of the jump in χ'' at $t = t_{w1} + t_{w2}$ is of the same order as the difference between the equilibrium values of χ''_{eq} at T_1 and $T_1 - \Delta T$. However, the time t_{erase} beyond which the stay at T_2 is erased does not conform to the naive estimate eq. (25), since it is found to be non monotonous and much larger than expected. It is rather the position t^* of the maximum of χ'' that seems to obey Eq. (25). Note that the REM scenario also predicts a monotonously decreasing recovery time t_{erase} with increasing ΔT . We have at present no physical interpretation for this discrepancy.

Although the experimental data is consistent with the above droplet/chaos interpretation, the present study shows explicitly that the non monotonous memory anomaly does not prove the existence of an overlap length (see also the discussion in [20] and in ref. [36]). Indeed, we argued that the REM trap model, where this overlap length is absent, is also able to reproduce qualitatively the memory anomaly if one works around the freezing temperature around which ‘temperature chaos’ effects are observed [30]. In the REM scenario, the positive contribution to the memory anomaly comes from an over concentration of the probability weight in deep traps at T_2 as compared to the equilibrium situation at T_1 (see the discussion in ref. [30]). Physically, this positive contribution corresponds to a freezing of small length scales at T_2 that have to unfreeze when back at T_1 , a scenario that was directly confirmed by the numerical simulations of [23] where temperature chaos is absent but rejuvenation and memory effects are clearly observed.

Acknowledgments

We wish to thank L. Berthier, J. Hammann, O. Martin and H. Yoshino for many useful conversations. M. S. acknowledges a fellowship from the French Ministry of research. M. S also would like to thank CEA Saclay for hospitality where main part of this work was performed. The LPTMS laboratory is an Unité de Recherche de l’Université Paris XI associée au CNRS.

Appendix

This appendix is devoted to explain in detail how we can calculate $Q(\tau, t)$. We assume that the probability $P_\alpha(t = 0)$ that the system is found at a state α at time $t = 0$ is given. For simplicity, let us first consider the case that the system is kept at a constant temperature T . It is easily found that $Q(\tau, t)$ is given as

$$Q(\tau, t)d\tau = \sum_{\beta, \alpha} d\tau \delta(\tau(\beta) - \tau) G_{\beta\alpha}(t) P_\alpha(t = 0), \quad (26)$$

where $G_{\beta\alpha}(t)$ is the Green function, i.e., the probability that the system which initially is at α reaches β at time t .

Now let us calculate the Green function. When the system which initially is at α reaches β at time t , there are the following two possibilities:

- (i) $\alpha = \beta$ and the system has not been activated during time t .
- (ii) The system is activated at t' ($< t$) and reaches β after that time.

In the case (ii), because the new state after the activation is chosen randomly from all the states, the probability that the system reaches β after the activation is $P_\beta^{\text{uni}}(t - t')$, where

$$P_\beta^{\text{uni}}(t) = \frac{1}{N} \sum_\gamma G_{\beta\gamma}(t), \quad (27)$$

and N is the number of states. Taking this fact into consideration and recalling that the system is activated from α with the probability $\tau(\alpha)^{-1}$, we obtain

$$G_{\beta\alpha}(t) = \delta_{\alpha\beta} \exp\left[-\frac{t}{\tau(\alpha)}\right] + \int_0^t \frac{dt'}{\tau(\alpha)} \exp\left[-\frac{t'}{\tau(\alpha)}\right] P_\beta^{\text{uni}}(t - t'). \quad (28)$$

The Laplace transformation of this equation leads us to

$$\begin{aligned} \hat{G}_{\beta\alpha}(s) &\equiv \int_0^\infty dt \exp[-st] G_{\beta\alpha}(t) \\ &= \frac{\tau(\alpha)\delta_{\alpha\beta}}{s\tau(\alpha) + 1} + \frac{\hat{P}_\beta^{\text{uni}}(s)}{s\tau(\alpha) + 1}, \end{aligned} \quad (29)$$

where $\hat{P}_\beta^{\text{uni}}(s)$ is the Laplace transformation of $P_\beta^{\text{uni}}(t)$. From this equation and the Laplace transformation of eq. (27), we find

$$\hat{P}_\beta^{\text{uni}}(s) = \frac{\frac{\tau(\beta)}{s\tau(\beta) + 1}}{\sum_\alpha \frac{s\tau(\alpha)}{s\tau(\alpha) + 1}}. \quad (30)$$

The calculation of $\hat{P}_\beta^{\text{uni}}(s)$ for small s and its inverse Laplace transformation have already been done in ref. [15]. The results are

$$\hat{P}_\beta^{\text{uni}}(s) = \begin{cases} \frac{\tau(\beta)}{Nxs^x c(x)(s\tau(\beta) + 1)} & (x < 1), \\ \frac{-\tau(\beta)}{Ns \log(s)(s\tau(\beta) + 1)} & (x = 1), \\ \frac{(x - 1)(s + 1)\tau(\beta)}{Nxs(s\tau(\beta) + 1)} & (x > 1), \end{cases} \quad (31)$$

and

$$P_{\beta}^{\text{uni}}(t) = \begin{cases} \frac{\int_0^t du u^{x-1} \exp[-(t-u)/\tau(\beta)]}{Nxc(x)\Gamma(x)} & (x < 1), \\ \frac{\tau(\beta)[1 - \exp[-t/\tau(\beta)]]}{\log(t)} & (x = 1), \\ \frac{(x-1)\tau(\beta)\{1 - \exp[-t/\tau(\beta)]\}}{Nx} & (x > 1), \end{cases} \quad (32)$$

where $x \equiv T/T_g$ and

$$c(x) = \Gamma(x)\Gamma(1-x) = \frac{\pi}{\sin(\pi x)}. \quad (33)$$

Now let us return to the calculation of $Q(\tau, t)$. The substitution of eq. (28) into eq. (26) leads us to

$$Q(\tau, t) = \exp[-t/\tau]Q(\tau, 0) + \int_1^{\infty} d\tau' \int_0^t \frac{dt'}{\tau'} Q^{\text{uni}}(\tau, t-t') e^{-\frac{t'}{\tau'}} Q(\tau', 0), \quad (34)$$

where

$$Q(\tau, 0)d\tau \equiv \sum_{\alpha} d\tau \delta(\tau(\alpha) - \tau) P_{\alpha}(t=0), \quad (35)$$

and

$$Q^{\text{uni}}(\tau, t)d\tau \equiv \sum_{\alpha} d\tau \delta(\tau(\alpha) - \tau) P_{\alpha}^{\text{uni}}(t) = d\tau N p_x(\tau) P^{\text{uni}}(\tau, t). \quad (36)$$

The function $p_x(\tau)$ is defined by eq. (3). From eqs. (32), (34) and (36), we finally obtain

$$Q(\tau, t) - \exp[-t/\tau]Q(\tau, 0) = \begin{cases} \frac{p_x(\tau)\tau}{xc(x)\Gamma(x)} \int_1^{\infty} d\tau' \int_0^t du u^{x-1} \frac{Q(\tau', 0)}{\tau' - \tau} \times \left[\exp\left(\frac{u-t}{\tau'}\right) - \exp\left(\frac{u-t}{\tau}\right) \right] & (x < 1), \\ \frac{p_x(\tau)\tau}{\log(t)} \int_0^{\infty} d\tau' Q(\tau', 0) \times \left[\{1 - e^{-\frac{t}{\tau'}}\} - \frac{\tau}{\tau' - \tau} \{e^{-\frac{t}{\tau'}} - e^{-\frac{t}{\tau}}\} \right] & (x = 1), \\ \frac{(x-1)p_x(\tau)\tau}{x} \int_0^{\infty} d\tau' Q(\tau', 0) \times \left[\{1 - e^{-\frac{t}{\tau'}}\} - \frac{\tau}{\tau' - \tau} \{e^{-\frac{t}{\tau'}} - e^{-\frac{t}{\tau}}\} \right] & (x > 1). \end{cases} \quad (37)$$

Next, let us consider how we can calculate $Q(\tau, t)$ when the temperature is changed discontinuously as

$$T(t) = T_i \quad (t_i \leq t \leq t_{i+1}). \quad (38)$$

The answer is rather simple. At first, we calculate $Q(\tau, t_{w1})$ with some initial distribution $Q(\tau, 0)$. Then, we set the new initial distribution to $Q(\tau, t_{w1})$ and use eq. (37) to calculate $Q(\tau, t_{w2})$. We can calculate $Q(\tau, t)$ at any t by repeating this procedure.

References

1. E. Vincent, J. Hammann, M. Ocio, J. P. Bouchaud and L. F. Cugliandolo: in *Proceeding of the Sitges Conference on Glassy Systems*, ed. E. Rubi (Springer, Berlin, 1996).
2. P. Nordblad and P. Svendlidh: in *Spin-glasses and random fields*, ed. A. P. Young, (World Scientific, Singapore, 1997).
3. M. B. Weissman: in the same book as in Ref. [2].
4. F. Lefloch, J. Hammann, M. Ocio and E. Vincent: *Europhys. Lett* **18** (1992) 647.
5. E. Vincent, J. P. Bouchaud, J. Hammann and F. Lefloch: *Phil. Mag. B* **71** (1995) 489.
6. J. O. Andersson, J. Mattsson and P. Nordblad: *Phys. Rev. B* **48** (1993) 13977.
7. V. Dupuis, E. Vincent, J.-P. Bouchaud, J. Hammann, A. Ito and H. A. Katori, *Phys. Rev. B* **64**, 174204 (2001).
8. F. Alberici, P. Doussineau and A. Levelut: *J. Phys. I (France)* **7** (1997) 329.
9. F. Alberich-Kious, J. P. Bouchaud, L. F. Cugliandolo, P. Doussineau and A. Levelut: *Phys. Rev. Lett.* **81** (1998) 4987.
10. P. Doussineau, T. Lacerda-Aroso and A. Levelut: *Europhys. Lett* **46** (1999) 401.
11. L. Bellon, S. Ciliberto and C. Laroche: preprint cond-mat/9905160.
12. B. Derrida: *Phys. Rev. B* **24** (1981) 2613.
13. B. Derrida and E. Gardner: *J. Phys. C* **19** (1986) 2253.
14. J. P. Bouchaud: *J. Phys. I France* **2** (1992) 1705.
15. J. P. Bouchaud and D. S. Dean: *J. Phys. I France* **5** (1995) 265.
16. M. Sasaki and K. Nemoto: *J. Phys. Soc. Jpn.* **69** (2000) 2283.
17. M. Sasaki and K. Nemoto: *J. Phys. Soc. Jpn.* **69** (2000) 2642.
18. M. Sasaki and K. Nemoto: *J. Phys. Soc. Jpn.* **69** (2000) 3045.
19. M. Sasaki and K. Nemoto: *J. Phys. Soc. Jpn.* **70** (2001) 1099.
20. J.-P. Bouchaud, V. Dupuis, J. Hammann and E. Vincent, *Phys. Rev. B* **65**, 024439 (2001).
21. P. E. Jönsson, H. Yoshino, P. Nordblad, H. Aruga Katori, and A. Ito, preprint cond-mat/0112389.
22. T. Komori, H. Yoshino and H. Takayama, *J. Phys. Soc. Jpn.* **68**, 3387 (1999); **69**, 1192 (2000); **69**, Suppl. A 228 (2000).
23. L. Berthier, J.P. Bouchaud, preprint cond-mat/0202069
24. K. Jonason, E. Vincent, J. Hammann, J.-P. Bouchaud and P. Nordblad, *Phys. Rev. Lett.* **81**, 3243 (1998).
25. For a recent work from a more mathematical point of view, see: G. Ben Arous, A. Bovier, V. Gayrard, *Aging in the random energy model*, preprint cond-mat/0110223.
26. K. Nemoto: *J. Phys. A* **21** (1988) L287.
27. M. Picco, F. Ricci-Tersenghi and F. Ritort: *Phys. Rev. B* **63** (2001) 174412.
28. M. Picco, F. Ricci-Tersenghi and F. Ritort: *Eur. Phys. J. B* **21** (2001) 211.
29. J.-P. Bouchaud, in *Soft and fragile matter*, Eds.: M. E. Cates and M. R. Evans (Institute of Physics Publishing, Bristol, 2000).
30. M. Sales, J.P. Bouchaud, *Europhys. Lett.* **56** 181 (2001).
31. Ph. Refregier, E. Vincent, J. Hammann and M. Ocio, *J. Phys. France* **48**, 1533 (1987)
32. D. S. Fisher and D. A. Huse, *Phys. Rev. B* **38**, 373 (1988).

33. A. J. Bray and M. A. Moore, *Phys. Rev. Lett.* **58**, 57 (1987).
34. H. Yoshino, A. Lemaître, and J.-P. Bouchaud, *Eur. Phys. J. B* **20**, 367 (2001).
35. H. Yoshino, K. Hukushima, H. Takayama, preprint cond-mat/0203267
36. P. E. Jönsson, H. Yoshino, P. Nordblad, preprint cond-mat/0203444.
37. A. J. Kovacs, *Adv. Polym. Sci.* **3**, 394 (1963); A. J. Kovacs *et al.*, *Journal of Polymer Science* **17**, 1097 (1979).